ISSN 1828-5961

Using video for reconstruction in SfM. The Capo d'Omo Tower on Mount Argentario

In the context of 3D surveying methods, the role of drones is growing in importance. The capacity to approach the object and acquire both photos and videos from points that are highly inaccessible from the ground make these devices an efficient tool on the architectural and territorial scales, whether anthropized or not. Even more widespread are so-called unmanned aircraft systems (UAS), inoffensive and lighter than 250 g, due to the simplification of the related standards and continued improvements in their acquisition devices. The most advanced photo-modelling programs are now able to process video clips directly, automatically selecting the photos suitable for input in scale-invariant feature transform (SIFT) and speeded up robust features (SURF) algorithms, essential aspects of structure from motion (SfM). This technological progress constitutes a significant jump in automating SfM investigations, especially when made with UAS. With this background, the case study presented here is the sighting tower of Capo d'Omo, situated atop Mount Argentario near Grosseto. Two questions are addressed: assessment of the metric reliability of a model automatically reconstructed from video clips (in this case, taken from an UAS) through comparison with a model acquired from an active sensor device; and a study of its potential and possible use in the SfM workflow, also considering the limited software and hardware requirements necessary to process this type of product.

Fabio Lanfranchi
Architect, Ph.D., Associate Professor at the DSDRA of 'Sapienza' University of Rome. He carries out an intense research activity that transversally embraces the following topics: architectural drawing and surveying; documentation issues peculiar to graphical aspects of historical Architecture design; experiences in the integration of surveying techniques.

Piero Barlozzini
Architect, Ph.D., Associate Professor in the DiBT at the University of Molise. Teaches courses on architectural representation and digital graphics. Undertakes research in the field of architectural heritage with a particular interest in documentation, analysis, 3D survey and modelling, communication.

Luca Martelli
Ph.D. student at the Department of History, Representation and Restoration of Architecture (DSDRA) of 'Sapienza' University of Rome. His main concentrations are: architectural and urban surveying; colour management processes in integrated surveying; the influence of colours on spatial perception; the theory of shadow representation.

Keywords:
SfM from aerial video; Ultralight UAS; Architectural analysis; Validation accuracy Capo d'Omo

DOI: https://doi.org/10.20365/disegnarecon.30.2023.6

ISSN 1828-5961

INTRODUCTION

Digital modelling for architecture and the landscape has benefited enormously from the introduction of structure from motion (SfM) techniques, in which speeded up robust features (SURF) and scale invariant feature transform (SIFT) algorithms play an essential role (Resch et al., 2015). The automatic determination of homologous points between photographs (Tuytelaars and Mikolajczyk, 2007) now allows 3D point clouds to be generated from unorganized collections of digital photographs (Agarwal et al., 2011; Snavely et al., 2008). In SfM processing, the refinement of the statistical calculation is not key since the parameters guiding it remain open and may be influenced by other factors, such as the type of optical sensor. Comparing the results obtained using a full frame (FF) camera with those that can be obtained from a contemporary compact digital video camera, we note that in the latter, the identification of homologous points is more fluid and linear, in exchange for a lower sampling resolution and lower focusing and illuminating quality. This result is not only due to the greater number of images that can usually be extracted from the films and the consequent improved continuity between photographs; indeed, the lower resolution involved in the step from camera to video camera corresponds to a simplification of the mathematical/statistical problem that the SURF and SIFT algorithms must address, thus lending the processing greater robustness at the expense of detail. When using unmanned aircraft systems (UAS), this possibility of carrying out SfM processing from video clips is particularly important and allows the technical evolution of photo-modelling to be summarized in three distinct moments:

- the introduction of the first UAS models, capable of taking individual photos during flight;
- the growing spread of UAS models capable of recording video, from which users can extract the photos deemed most suitable for SfM;
- technological advances in photo-modelling software, which is now capable of directly importing films by autonomously selecting the photos suitable for reconstructing a digital model statistically estimated to be the most plausible.

The evolution of software has significantly increased the automation of reconstruction using photo-modelling, presenting several opportunities as well as several questions, especially as to the reliability of the results. The necessary accuracy for acquiring and processing the data differs depending on the purpose of the product. For example, the required reliability of a 3D model for augmented reality (AR) cannot be compared to what is necessary for archaeological monitoring or the conservation and restoration of the architectural heritage. In civil fields, aerial photographic acquisition in single shots is aimed at SfM reconstruction and has long been widely documented with respect to the procedure and metric reliability of the models. Studies conducted in architecture (Grenzdörffer et al., 2015; Russo et al., 2022) and archaeology (Adami et al., 2019; Barba et al., 2019) have shown the metric reliability of SfM models with data acquired using active sensor devices oriented using total stations (TS) or the Global Navigation Satellite System (GNSS). With this background, this paper investigates the opportunities and/or limits inherent in automatic photo reconstruction, an operation that is offered by various developers today. The case study presented is the Capo d'Omo tower (Fig. 1), one of the numerous rectangular coastal observation towers in Italy, and particularly Mount Argentario in Tuscany. The demanding orographical context (Fig. 2), the reduced volume (about 8 m xm 8 m at the base by 8 m high), and the irregular partition walls presented the opportunity to use ultralight

Fig. 1 – Approach to the tower from the south-west crest and aerial views from the south and west.

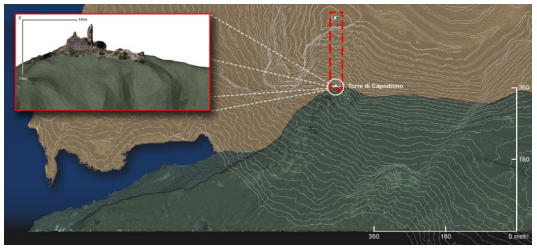

Fig. 2 – Drawing made from processing orthophotos of LIDAR point clouds from the 2009 Extraordinary Remote-Sensing Environmental Plan (Piano Straordinario di Telerilevamento Ambientale, PST-A), with an integrated nadiral view with equidistant lines and orthophoto with vertical frame from the south. In the inset, an image of the mesh model integrated and processed using aerial SfM and LIDAR data.
Source: LIDAR data from panels C42381108_0202 and C42381110_0202 from the 2009 Extraordinary Remote-Sensing Environmental Plan – ©Italian Ministry of Environment and Energy Security, Geoportale Nazionale – (2008). All Rights Reserved.

UAS and SfM to in vestigate the potential of a digital model processed automatically from video. The aim of the study is to determine the geometric/dimensional reliability of the model, assessing the possible opportunities to use it as both an end and a means, for example, as a finished product destined for communication or an auxiliary tool useful for the SfM workflow.

CASE STUDY AND HISTORICAL/GEOGRAPHICAL CONTEXT

This contribution focuses on a medieval tower pertaining to the fortified system of Mount Argentario, which is located on the western coast of the Tuscan promontory atop a cliff at about 350 metres above sea level. It is an isolated construction with a small rectangular base — about 8 m x 8 m — known as the Capo d'Omo tower, made of rubble masonry walls with strings of blocks made of local stone. Its purpose was to offer a key point of observation for soldiers charged with guarding the stretch of sea around the promontory, as well as allowing them to notifying the garrison protecting the area of the arrival of enemy ships (Luisi,

DOI: https://doi.org/10.20365/disegnarecon.30.2023.6

ISSN 1828-5961

1979). The archival sources on this tower are rather sparse. Observing the drawings of similar, contemporary structures in the territory (Della Monaca et al., 2000), we assume that this building was organized on two or three levels, with intermediate wooden floors, a vaulted masonry roof, and sighting terrace. For security, the entrance was located on the first level, and therefore reachable via a wooden ladder that could be easily removed. Today, only the base and part of the south-east façade remain, both of which are greatly damaged the base volume, with a truncated pyramid shape, features a scarp inclination of 13°. The structure is delimited at the top by a rather pronounced toroid-shaped oversailing course, only a small part of which is present today, coinciding with the height of the first floor level and the marked vertical faces. Within the volume, two rooms are defined by a barrel vault and a well — currently filled with detritus — probably used to contain food provisions and rainwater from the roof (Licinio, 1994). Remaining attached to the tower are the remains of another vaulted construction whose purpose is difficult to ascertain and — visible in the aerial images (Fig. 13) — the wall built on the edge of the plain towards the east, which probably protected the entrance. The Capo d'Omo tower was probably erected between the fifteenth and sixteenth centuries during the reign of the Republic of Siena over Mount Argentario (Fig. 3). Its construction was promoted during the reinforcement of a network of coastal towers that began in the ninth century following incursions by pirates and the Saracens (Cassi Ramelli, 1964). In 1557, after a military defeat, territories overseen by the Republic of Siena fell under the government of Cosimo I de' Medici, who aligned himself with the crown of Spain. In agreements with allies, Philip II of Spain, the suc In 1557, after a military defeat, territories overseen by the Republic of Siena fell under the government of Cosimo I de' Medici, who aligned himself with the crown of Spain. In agreements with allies, Philip II of Spain, the successor of Charles V, reserved the small coastal band between Orbetello in Capalbio and part of the island of Elba, constituting the State of the Presidi.

Fig. 3 – The coastal defence structures of Mount Argentario in the XVII Century. High on the left: map of the whole State of Siena. (Florence State Archive, Piante dello Scrittoio delle Fortezze e Fabbriche, ID 9.

Pianta di tutto lo Stato di Siena, XVII Sec., plant, 20 Italian miles, 765x730 mm, paper, china and watercolor.

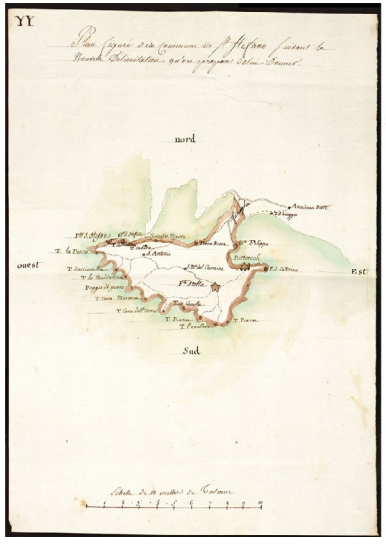

Plan figuré de la Commune de St. Stefano suivant la nouvelle delimitation qu'on propose de lui donner, 1809, plant, 10 Tuscan miles, 363x260 mm, paper, china and watercolor.

Fig. 4 – The coastal towers of Mount Argentario in the XIX Century. (Siena State Archive, French Gov., ID 8.)

During the decade of his mandate (1559–1571), the Viceroy of Naples, the Iberian Pedro Afán de Ribera, improved the military characteristics of this land under the impulse of Philip II to adapt it to the needs imposed by new weapons, renovating the network of coastal towers and building numerous strong fortresses (Faglia, 1974) (Fig. 4). Today, these military posts are a characteristic element of the Tuscan coast, testifying to the history and culture of Italy. Their protection assumes deep knowledge, passing through architectural surveying, enhancement, and a greater use while respecting their architectural and material specifics, as well as the territory where they were built.

MEANS OF ACQUISITION AND PROCESSING 3D DATA AND THE DEVICES USED

To investigate the potential of the SfM model to process film clips, a workflow was planned. This was organized into the three stages summarized in (Table 1): acquisition, processing, and integration and verification. For the campaign, 3D acquisition devices with active and passive sensors were used. Both the resulting photos and the point cloud recorded with a terrestrial laser scanner (TLS) were oriented on a common network of reference defined with a TS and aimed at comparing and assessing the SfM models obtained. The data, acquired using video cameras on the UAS and cameras on the ground, were oriented at points recorded with the TS for comparison with those taken using the TLS for the purposes of metric validation and multi-scale accuracy. The acquisition with the passive sensor was organized into two stages. The first was aimed at digitally reconstructing the tower as a whole using aerial film clips taken from the UAS. The second, made exclusively with snapshots from the ground was aimed at developing the more detailed digital model of the tower. With respect to hardware, an ST Leica TCR703 was used for the topographic survey, while the TLS acquisitions were made with a 3D laser scanner, FARO Focus M70 (Fig. 5). Aerial shots were taken with a DJI Mini 2 UAS equipped with a camera with 1/2.3" sensor mounted on an

DOI: https://doi.org/10.20365/disegnarecon.30.2023.6

ISSN 1828-5961

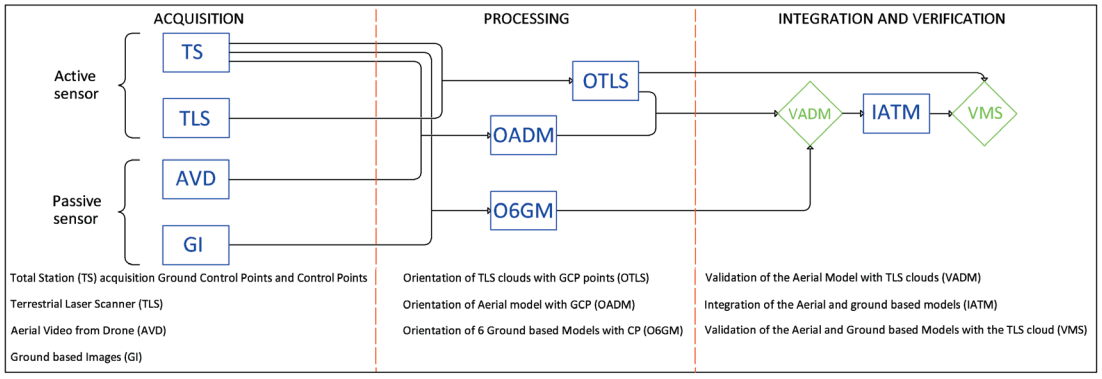

Table 1 – Diagram of the workflow.

electronically stabilized gimbal with: maximum resolution 12 MP; focal length 24 mm; aperture f2.8; ISO 100; automatic white balancing; resolution 1920 pixels x 1080 pixels. For photos taken from the ground, a digital Nikon D850 camera was used with: CMOSFX image sensor 35.9 mm x 23.9 mm; maximum resolution 45.7 MP; objective 58 mm; aperture f8; ISO 100; manual white balancing; resolution 6192 pixels x4128 pixels (Fig. 6). With regard to software, the photogrammetric models were processed using 3DF Zephir® v. 7.013 by 3DFLOWSrl; the digital TLS model was built using JRC Recostructor® v. 4.3.2 by Gexel; the films were edited using the open source video editor Shotcut v. 23.06.14; and the comparative drawings were produced with the open source software CloudCompare v. 2.11.3.

Fig. 5 – Active sensor devices used for the acquisition campaign. The high-visibility A4 target is on the ground for shots taken from the drone.

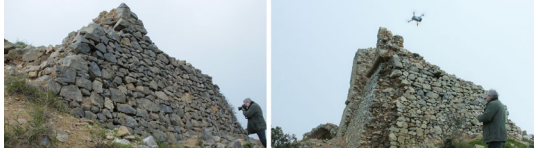

Fig. 6 – Passive sensor devices used for the aerial and ground-based acquisition campaign.

DATA ACQUISITION AND PROCESSING USING ACTIVE SENSOR DEVICES, TOPOGRAPHICAL NETWORK, AND TERRESTRIAL LASER SCANNING

The non-oriented topographical network, organized on the basis of tacheometry, was used as a common system of reference for acquiring both the aerial/ground-based photos and TLS.
The five station points, four of which were positioned outside and one inside the grounds of the construction (Fig. 7), define the vertices of the closed non-oriented polygon and were used as limits on the ground and ground control points (GCP) in the process of orienting the aerial SfM model. An integral part of the network involved another 26 points collimated on the construction, which were used as limits and control points (CP) for the ground-based SfM and TLS models (Fig. 8). When selecting the points, particular attention was paid to covering the entire construction and given the particular orography of the site, this

Fig. 7 – Aerial view of the tower. The targets situated at the TS points are on the ground.

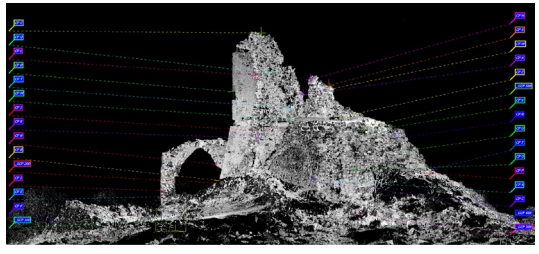

Fig. 8 – Set of TLS point clouds with reflectance values and points used when defining the models.

practice was essential during the digital reconstruction to minimize both the overall alignment errors and possible imprecision (mixed pixels) typical of acquisitions made from faraway, protected centres of projection (Litchi, 2007: 307-324; Wang and Cheng, 2016: 246-258). Both for the reasons above and due to the dimensions of the typical precise polygon (i.e. with the extension of the individual sides between about 6 and 11 m), the TS and reflecting prism were placed with forced centring to localize possible eccentricity errors in the individual stations, minimizing the angular

DOI: https://doi.org/10.20365/disegnarecon.30.2023.6

ISSN 1828-5961

propagation.
The polygon was verified using the field measurements, by checking both the spatial coincidence between the same control points acquired from different stations and the coincidence between the last point collimated by final station 500 and initial station 100. The second acquisition phase with active sensor regarded the 3D terrestrial laser scan dedicated to controlling the accuracy of the SfM models. Despite the modest size and weight of the laser scanner, the rough orography of the site (especially for the southern face situated just behind the cliff) did not allow for positioning at the best points. The TLS campaign was carried out with six scans for a total of more than 200 million acquired points (Fig. 9).
With regard to the acquisition features and the scanned area:
• two were set with a resolution of 7.7 mm at 20 m and used to document the eastern environment, which includes the broad plain from which the tower was probably accessed and which today has the only part that remains standing, in addition to the vault against the base;
• two were set with a resolution of 7.7 mm at 10 m and made on the norther and southern faces and the ground within the tower, coinciding with the string course at the top of the connection between the ground and construction;
• two scans were made with a resolution of 3 mm at 5 m for the western face, which were also aimed at comparing the reconstruction results on the detailed level of the masonry wall facing, defined through three different processing models.
Once the anomalous values — for example duplicate and inconsistent points — were removed to reduce the calculation uncertainties, the point clouds were aligned one at a time with the iterative closest point (ICP) procedures with reference to the GCP and CP targets. To reduce the overall alignment error, given the satisfactory intervisibility of different areas among scans and the sparse vegetation moved by the wind, the clouds were processed using bundle optimization methods, the overall alignment error of which was equal to 0.2 mm.

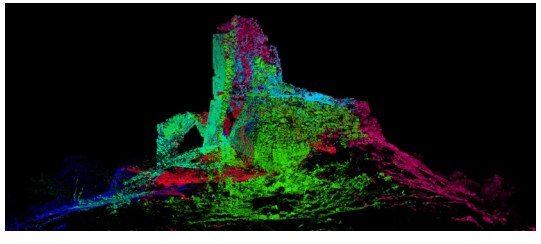

Fig. 9 – View of the gamma maps of the six TLS scans.

DATA ACQUISITION AND PROCESSING USING AERIAL AND GROUND-BASED PASSIVE SENSOR DEVICES

For the UAS video campaign, three missions were carried out. One was dedicated to nadiral acquisition in programmed flight mode (waypoint). The other two were done via manual control of the UAS with the objective of acquiring elevations. These were designed to optimize the percent coverage between frames in relation to both the frequency of frames per second (fps) chosen for the films, i.e. 30 fps, and the speed of the drone. The missions involved five revolutions around the construction, set at camera distances, heights, and orientations suited to the elevations and the terrain (Fig. 10). After 'cuts' were made to remove parts not useful for the photo-modelling, the three films were combined into a single MP4 film with a size of 2.59 GB and a duration of 8:34 minutes. To assess the automatic photo reconstruction capabilities of the software, any correction to the parameters of the input films was avoided. To minimize the orientation errors of the sparse cloud, determined using the 450 photos extracted by the software and consisting of nearly 100,000 points, an initial bundle adjustment was made using the five GCP stations in the topographic network. With regard to the model alignment values (Table 2), the maximum residual was 0.450 cm for the spatial vector relating to GCP 300. As for the XYZ components, the maximum residual was 0.412 cm in the Y direction (roughly parallel to the western side), also for GCP 300. The final average residual (FAR) was

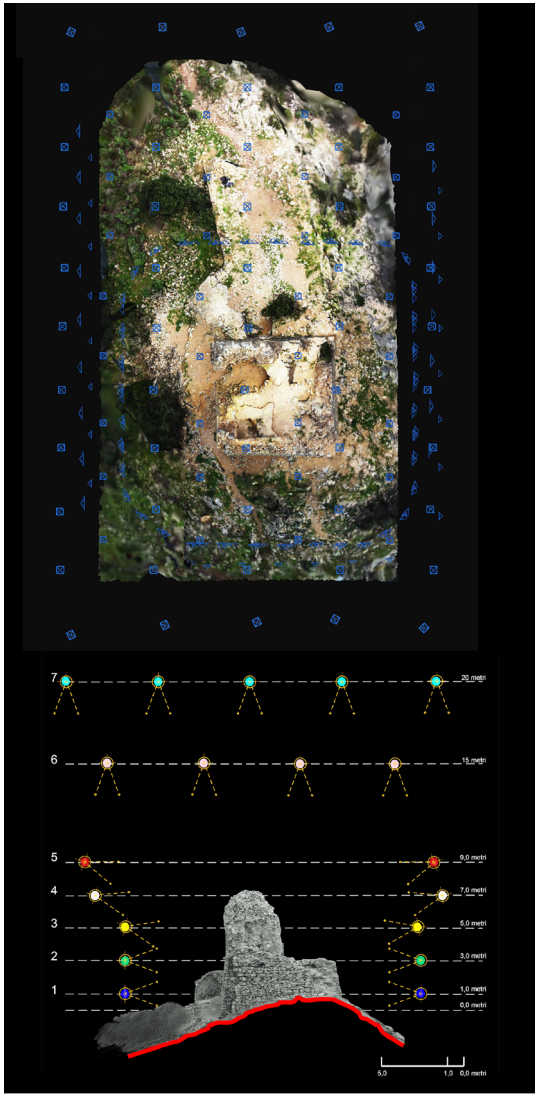

Fig. 10 – Above, nadiral view of the model with snapshot points extracted from the films. Below, the diagram of planned flight heights for video acquisition.

DOI: https://doi.org/10.20365/disegnarecon.30.2023.6

ISSN 1828-5961

Point code (GCP)	X error (cm)	Y error (cm)	Z error (cm)	Final residue (cm)
100	0,05	0,05	0,00	0,07
200	0,05	0,18	0,15	0,24
300	0,07	0,41	0,16	0,45
400	0,18	0,13	0,01	0,22
500	0,01	0,14	0,00	0,14

Table 2 – List of final 3D residuals relating to the ground control points (GCP).

0.229 cm. The root mean squared error (RMSE) was equal to 0.261 cm. The acquisition of ground-based photographs was based on common cultural heritage surveying methods documented in the literature for more than 20 years (Hakim et al., 2003; Guidi et al., 2006; Reljic et al., 2019).
It should be noted, however, that in the situation discussed here, the different architectural/environmental contexts require a certain flexibility or even exceptions to consolidated methodological practice. In this case, the orography around the tower is very irregular and steep on two sides, in addition to a substantial impracticability on the south-west/southern face at the top of the Capo d'Omo cliff.
The inclination of the base contributed to making the photographic acquisition of the construction rather difficult and also made the adoption of tools such as telescopic rods to raise the photographic point impractical, thus hampering the correct definition of the upper parts of the construction. From the operational point of view, the ground-based photographic campaign was strategically organized around reordering the snapshots (Barba et al., 2019).
Of the 1618 total images acquired, 934 were used to define the sparse cloud. To optimize the metric results, the camera was self-calibrated in the post-processing phase (Remondino and Fraser, 2006) and the software was used to select individual photos based on the best intrinsic characteristics. The set of snapshots was divided into six datasets corresponding to the four different faces and local areas, such as the vault and ground at the top of the scarp, integrated with the rear part of the partition wall in the residual elevation. Having defined the related sparse clouds, oriented for each dataset on the relative points, the resulting models were processed through bundle adjustment to reduce reprojection errors. From the alignment values drawn from the six different models oriented on the GCPs and CPs, a maximum FAR of 0.082 cm was obtained, with an RMSE equal to 0.084 cm for the dataset relating to the eastern/south-east face, collimated from station 200 (Fig. 11).

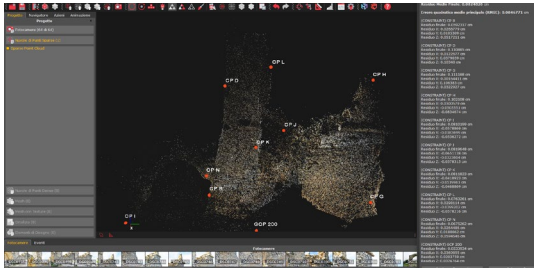

Fig. 11 – Screenshot of the sparse cloud of the eastern/south-eastern face with alignment values.

VERIFYING THE CONGRUENCE AND RELIABILITY OF THE AERIAL PHOTOGRAMMETRIC MODEL

The overall comparative analysis of the aerial SfM million was carried out using the Cloud Compare software. The dense cloud, consisting of little more than 2 million points, was compared with the union of TLS clouds reduced to a number of points similar to that in the photogrammetric model.
The scale of colours generated indicates deviations between 0 and 30 cm. With regard to the masonry, the comparison shows good agreement between the models, with average deviations less than 2 cm and maximum deviations less than 5 cm (Fig. 12).
The most significant variations, as shown by greens and yellows, occur for the walls affected by vegetation, even in the partitions themselves.
Zones with further deviations include poorly lit and/or faraway areas, such as the intrados of the vault, and the upper areas, such as the top of the elevation wall.
Given the results of the metric comparison, the aerial SfM method definitively revealed good reliability, even considering the orientation method used. In fact, to orient the TLS cloud, all the available topographic points were processed, while for the aerial photogrammetry cloud, only the GCPs were use, although the full list of all collimated points was also inserted in the model. With regard to agreement in terms of visually rendering the materials, this was, as expected, different. The video camera sensor incorporated in the UAS is not comparable to the one in the FF camera used. Momentarily overlooking this aspect, an initial series of considerations can be presented.

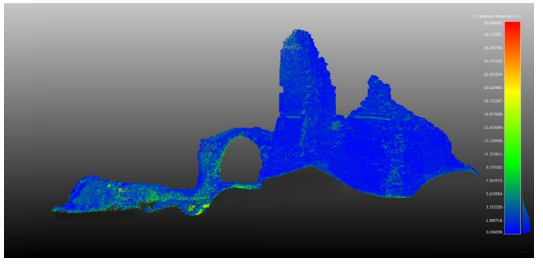

Fig. 12 – Map of deviation between the TLS clouds and aerial photogrammetry cloud..

The deviations between TLS and aerial clouds indicate good overall agreement. These values are largely below the margins of uncertainty or conventionally allowed indetermination for graphical rendering on the 1:100 scale, remaining acceptable even for the 1:50 scale. To optimize the orientation of the aerial model, even for its possible use in the conventional SfM workflow, all available control points were interpolated, as were those used for orientation via bundle adjustment. Even in this case, the maximum residual RAF and RMSE deviations obtained after bundle adjustment confirmed alignment values similar to those found previously.

INTEGRATION OF THE AERIAL SFM CLOUD AND GROUND-BASED CLOUDS, COMPARISON AND VERIFICATION OF AGREEMENT AND RELIABILITY

The integration between the aerial photogrammetric model considered as a reference and the

DOI: https://doi.org/10.20365/disegnarecon.30.2023.6

ISSN 1828-5961

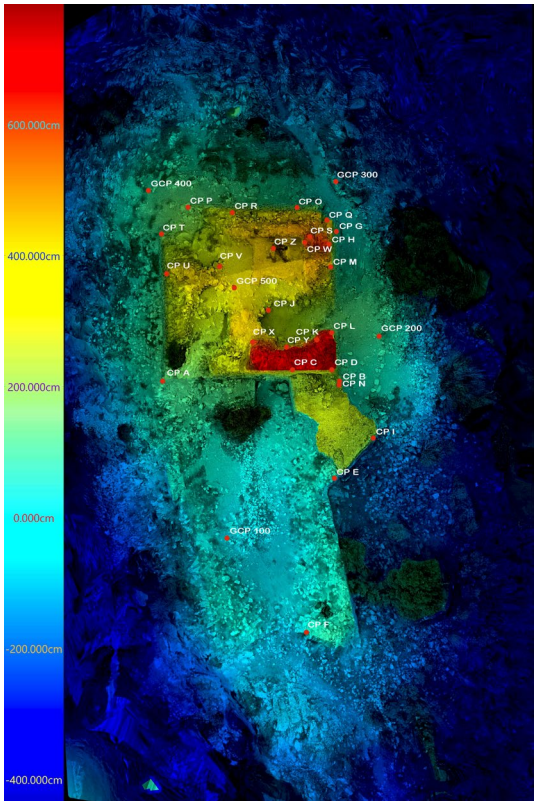

Fig. 13 – Orthophoto of the tower and its immediate surroundings, with an indication of the control points used for alignment. The image shows the chromatic range relating to the heights.

six ground-based models was made through direct combination, using the local common system of reference (Fig. 13). The alignment values calculated for the complete model, defined using 1384 aerial and ground-based photos consisted of an FAR of 0.009 cm and an RMSE of 0.013 cm. For the overall reliability of the model, the dense cloud consisting of about 8 million points was compared with the TLS cloud with a similar density.
The results of the deviation between the surfaces of the models are reported in (Fig. 14) with an

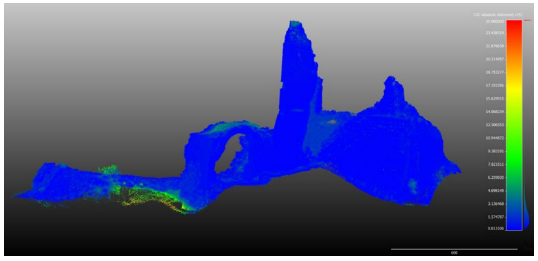

Fig. 14 – Map of deviation between the TLS clouds and aerial photogrammetry cloud.

Fig. 15 – Orthophoto of the plan extracted from the mesh model developed after integrating the ground-based and aerial images.

appropriate colour map. In this case as well, the most significant variations were due to the vegetation and local indeterminacies relating to the highest areas. The scale calculated by the software shows deviations between 0 and 25 cm.
In this case as well, the analysis shows good agreement among the different models, with absolute variations that do not exceed 4.5 cm.
The subsequent post-processing confirmed the good result of the integration, even in terms of surface rendering. The definition of the mesh model, developed using the dense cloud visible in (Fig. 15) and (Fig. 16), shows both the metric reliability and valid values of definition, also for representations on the detailed scale. (Fig. 17) shows a comparison of two parts of the mesh from the same orthophoto area.
On the right is the mesh from the ground-based photo and the left shows the mesh from the aerial video. Returning to the considerations mentioned above, the comparison clearly shows how, in contrast to the reliability seen for the dimensions, the model developed using the aerial video does not

Fig. 16 – Orthophoto of the four faces extracted from the mesh model developed after integrating the ground-based and aerial images.

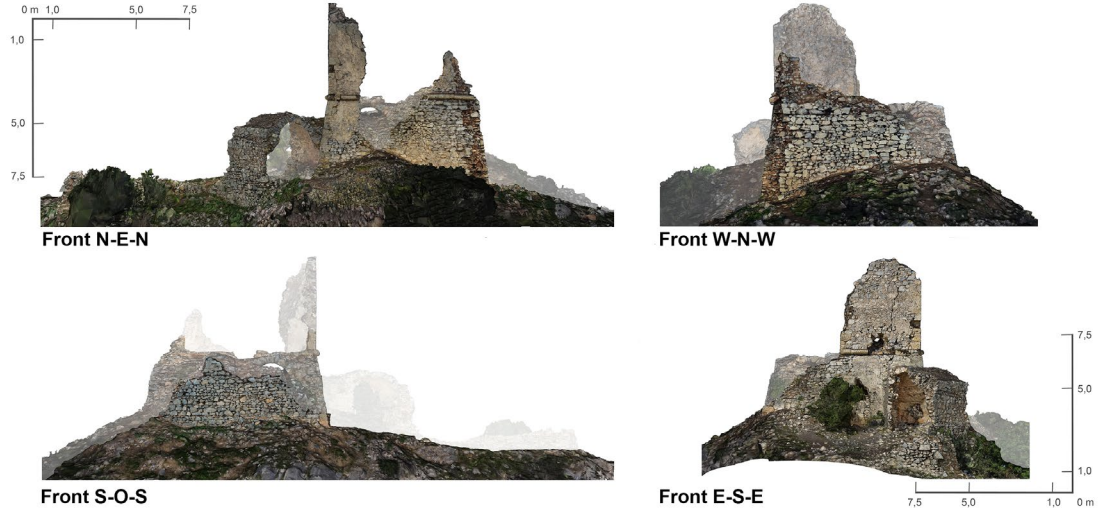

DOI: https://doi.org/10.20365/disegnarecon.30.2023.6

ISSN 1828-5961

Fig. 17 – Comparison of the meshes processed from the aerial (left) and ground-based (right) photogrammetric models.

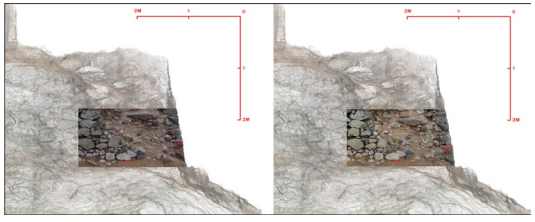

Fig. 18 – Representation in 1:50 scale of a façade and section of the tower.

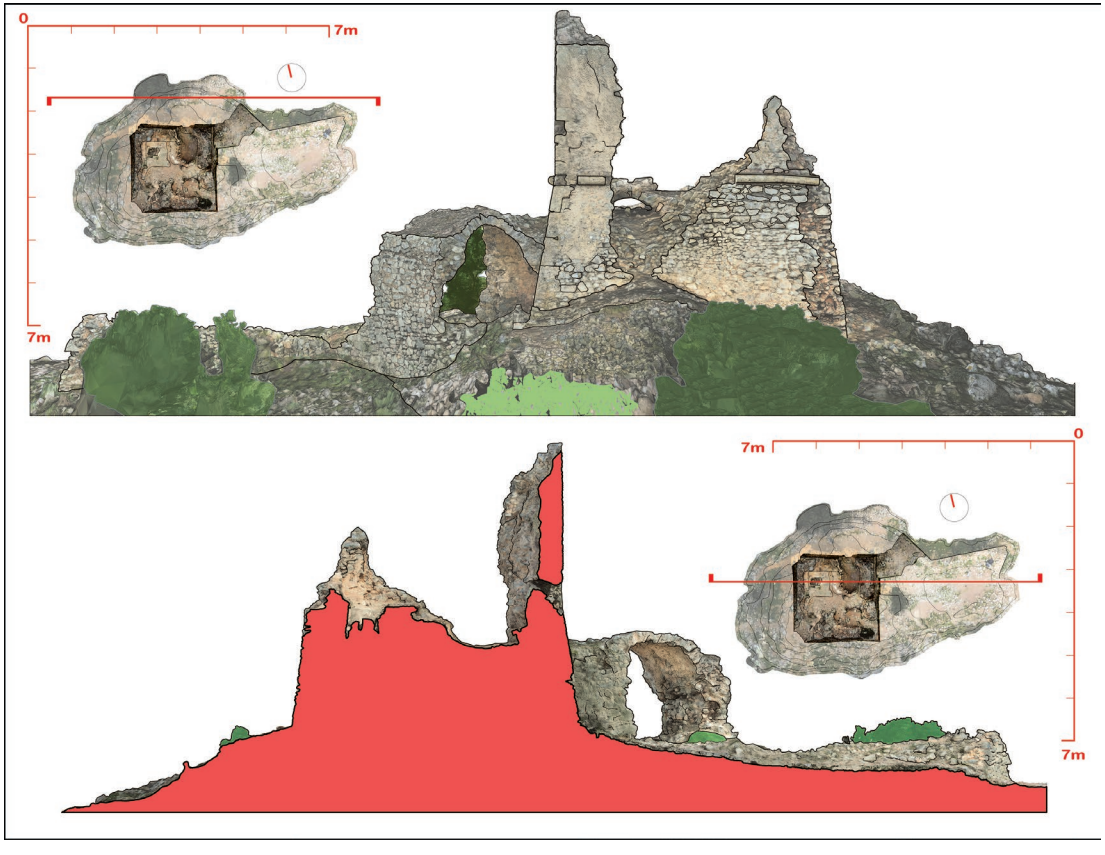

show a similar representational rigour.
As anticipated, the causes lie in the size and quality of the photographic sensor, which do not allow the colour depth values offered by larger sensors to be recorded and therefore interpreted. Despite the expected limits in terms of defining the surfaces on the detailed scale, the results of this experiment satisfy the initial hypotheses considering the resulting metric reliability, processing speed, and opportunity to provide a model useful for both the digital notation of data and possible communicational uses compatible with the level of definition obtained.
The SfM model generated from video therefore overcomes the alternative low-resolution concept with respect to the model developed from photographs with a higher resolution. The range of possible studies regarding both dimensions and complexity for potential insertion in the SfM workflow is thus expanded by these initial results. (Fig. 18) in 1:50 section shows the north-east/northern elevation and a longitudinal section of the tower. 'Traditional' two-dimensional drawings were made using CAD and rendered based on the orthophotos extracted from the integrated photogrammetric model.

CONCLUSION

When investigating an architectural object of modest size yet with a particular location and volumetric features, SfM photo-modelling may make valid use of a quick photogrammetric model that is automatically extracted and processed by the software.
This is valid in terms of both time to calculate the entire reconstruction and communication (for example, this model is suited to publication).
The experimental campaign focusing on defining a 3D model processed from videos taken with low-resolution cameras and incorporated in a UAS, produced a quick, reliable model with a definition suitable for dynamic publishing that can be divulged and open to integration with digital data acquired from other sources.
Therefore, starting with a product based on videos and automatically processed using software, the resulting model represented a useful means for recording digital data and also an effective tool useful for developing more advanced processing stages. In other terms, it is an 'active digital eidotype' providing the operator with an initial cognitive approach which is also useful for planning and initiating the subsequent phases of work.
There is a clear awareness that the procedures presented here require additional tests to refine the proposed method for constructions of a similar size, but especially for architecture on a larger

DOI: https://doi.org/10.20365/disegnarecon.30.2023.6

REFERENCES

Adami, A., Fregonese, L., Gallo, M., Helder, J., Pepe, M., and Treccani, D. (2019). Ultra light UAV sys-tems for the metrical documentation of Cultural Heritage: applications for architecture and archeology. In Int. Arch. Photogramm. Remote Sens. Spatial Inf. Sci. (vol. XLII-2/ W17, 15–21). Gottinga: Copernicus Publications.

Agarwal, S., Furukawa, Y., Snave-ly, N., Simon, I., Curless, B., Seitz, S., Szeliski, R., (2011). Communica-tions of the ACM, October 2011, Vol. 54 No. 10, 105-112

Barba, S., Barbarella, M., Di Bene-detto, A., Fiani, M., Gujski, L., Li-mongiello, M., (2019). Accuracy As-sessment of 3D Photogram-metric Models from an Unmanned Aerial Vehicle. In: Drones 3, no. 4: 79. MDPI: Basel.

Cassi Ramelli, A. (1964). Dalle cav-erne ai rifugi blindati. Trenta secoli di architettura militare. Milano: Nuova Accademia Editrice.

della Monaca, G., Roselli, D., Tosi, G. (2000). Fortezze e torri costiere dell'Argentario, Giglio e Giannutri Cronaca Storia Aspetti architetton-ici, Pittigliano: Laurum Editrice.

El-Hakim, S., Beraldin, J-A., Picar, M., Vettore, A., (2003) Effective 3D Modeling of Heritage Sites. In: 4th International Conference of 3D Imaging and Modeling (3DIM'03). 302-309.

Faglia, V. (1974). La difesa anti-corsara in Italia dal XVI secolo. Le torri costiere e gli edifici rurali fortificati. Roma: Istituto Italiano dei Castelli.

Grenzdörffer, G. J., Naumann, M., Niemeyer, F., Frank, A., (2015). Symbiosis of UAS photogramme-try and TLS for surveying and 3D modeling of cultural heritage mon-uments – A case study about the Ca-thedral of St. Nicholas in the city of Greifswald. In: International Archives of Photogrammetry, Re-mote Sensing and Spatial Informa-tion Sciences, XL-1/W4 (1), 91–96.

Guidi, G., Frischer, B., Russo, M., Spinetti, A., Carosso, L., Micoli, L.L., (2006). Three-dimensional acqui-sition of large and detailed cultural heritage objects. In: Ma-chine Vision and Applications. Am-sterdam: Elsevier, 17 (6), 349-360.

Lichti, D.D., (2007). Error model-ling, calibration and analysis of an AM–CW terrestrial laser scanner sys-tem. ISPRS Journal of Photo-grammetry and Remote Sensing, 61(5), 307-324.

Licinio, R. (1994). Castelli medieva-li. Puglia e Basilicata: dai Normanni a Federico II e Carlo I d'Angiò. Bari: edizioni Dedalo.
Published proceedings: Author, A., & Author, B. (2016). Title. *In Pro-ceedings of UID* (vol. 20, pp. 10-20). City: Publisher.

Luisi, R. (1979). Scudi di pietra I castelli e l'arte della guerra tra Me-dievo e Rinascimento. Roma-Bari: Edi-tori Laterza.

Remondino, F.; Fraser, C., (2006). Digital camera calibration meth-ods: Considerations and compar-isons. In: International Archives of the Photogrammetry, Remote Sensing and Spatial Information Sciences. V. 36, no. 5, 266.-272.

Reljic, I., Duncer, I., & Seljan, S. (2019). Photogrammetric 3D scan-ning of physical objects: tools and workflow. TEM Journal, 8(2), 383-388.

Resch, B., Hendrik, P., Lensch, A., Wang, O., Pollefeys, M., Sork-ine-Hornung, A., (2015). Scalable Struc-ture From Motion for Dense-ly Sampled Videos. Proceedings of the IEEE Conference on Computer Vi-sion and Pattern Recognition (CVPR), 3936-3944.

Russo, M., Panarotto, F., Fleng-hi, G., Russo, V., Pellegrinelli, A., (2022). Ultralight UAV for steep-hill ar-chaeological 3D survey. In: Disegnare con, v. 15, no. 29.

Snavely, N., Seitz, S. M., Szeliski, R., (2008). Modeling the world from internet photo collections. IJCV, 80(2): 189–210.

Tuytelaars, T., Mikolajczyk, K., (2008). Local Invariant Feature De-tectors: A Survey. Foundations and Trends® in Computer Graphics and Vision: Vol. 3: No. 3, 177-280.

Wang, Q., Cheng, J., (2016). Devel-opment of a mixed pixel filter for improved dimension estimation us-ing AMCW laser scanner. ISPRS Journal of Photogrammetry and Remote Sensing. 119, 246-258.

DOI: https://doi.org/10.20365/disegnarecon.30.2023.6